JGR Planets

RESEARCH ARTICLE
10.1029/2021JE007007

Key Points:

- We present a complete mapping of a large vent population in the Arcadia Planitia region of the northern plains of Mars
- We reconstructed the subsurface mechanical layering underlying the vent field using spatial distribution analysis
- These analyses proved to be efficient and open the possibility of collecting subsurface rheological data from areas beyond InSight reach

Supporting Information:

Supporting Information may be found in the online version of this article.

Correspondence to:

B. De Toffoli,
Barbara.Detoffoli@dlr.de

Citation:

De Toffoli, B., Massironi, M., Mazzarini, F., & Bistacchi, A. (2021). Rheological and mechanical layering of the crust underneath thumbprint terrains in Arcadia Planitia, Mars. *Journal of Geophysical Research: Planets*, *126*, e2021JE007007. https://doi.org/10.1029/2021JE007007

Received 21 JUL 2021
Accepted 19 OCT 2021

Author Contributions:

Conceptualization: B. De Toffoli
Formal analysis: B. De Toffoli, F. Mazzarini
Funding acquisition: M. Massironi
Investigation: B. De Toffoli
Methodology: F. Mazzarini, A. Bistacchi
Project Administration: M. Massironi
Software: F. Mazzarini, A. Bistacchi
Supervision: M. Massironi
Validation: M. Massironi
Visualization: B. De Toffoli
Writing – original draft: B. De Toffoli

Rheological and Mechanical Layering of the Crust Underneath Thumbprint Terrains in Arcadia Planitia, Mars

B. De Toffoli[1,2], M. Massironi[2,3], F. Mazzarini[4], and A. Bistacchi[5]

[1]German Aerospace Center (DLR), Institute of Planetary Research, Berlin, Germany, [2]Department of Geosciences, University of Padova, Padova, Italy, [3]INAF, Osservatorio Astronomico di Padova, Padova, Italy, [4]Istituto Nazionale di Geofisica e Vulcanologia, Pisa, Italy, [5]Dipartimento di Scienze dell'Ambiente e della Terra, Università degli Studi di Milano-Bicocca, Milan, Italy

Abstract In the area of Arcadia Planitia in the Northern hemisphere of Mars, mounds indicating fluid and sediment emissions have been already recognized. Here, we show that through fractal and fracture-spacing analyses of a large vent population it is possible to infer the mechanical layering of the underlying subsurface. Our work includes the mapping of an entire population of 9,028 vents over an area of 122,000 km^2. The analysis of mound distribution at the surface led to the formulation of inferences about the subsurface feeding conduits, and to the identification of three mechanical discontinuities at c. 4–5, c. 14–23, and c. 50–55 km. This evidence matches the mechanical stratigraphy recorded by the InSight NASA mission, and is in agreement with independent previous subsurface global modeling, supporting our conclusions.

Plain Language Summary The Martian northern hemisphere displays mounds interpreted to be the result of sediment and water erupting onto the surface. We analyzed the mounds spatial distribution and found patterns that reflects the extent at depth of the subsurface conduits that fed those mounds (array of fractures, i.e., high permeability pathways) allowing the sediment and water upwelling. These conduits thus connect the surface to the source of the erupted materials at depth. These source levels are located at the base of layers characterized by mechanical properties different from the adjacent ones (e.g., loose sediments vs. crystalline bedrock). Such layers are hence referred as mechanical discontinuities. We identified three discontinuities: at c. 4–5, c. 14–23, and c. 50–55 km. Our outcomes match the mechanical stratigraphy recorded by the InSight NASA mission, and is in agreement with independent previous subsurface global modeling, supporting our conclusions.

1. Introduction

We studied the area of Arcadia Planitia, a portion of the Martian northern lowlands, or "Vastitas Borealis," located at mid-high latitudes (51°N 177°E) and around 4 km below the mean Martian elevation (Figure 1) where a large vent field has been proposed (De Toffoli et al., 2019). This area is characterized by two geological units: the Vastitas Borealis (a) marginal and (b) interior units. These are interpreted as the product of an Early Amazonian pervasive alteration of sediments emplaced during outflow events in the Late Hesperian. These deposits were sporadically covered by ejecta blankets from Amazonian craters (e.g., Tanaka et al., 2005, 2014). We investigated non-random alignments of sedimentary volcanoes covering part of Arcadia Planitia (De Toffoli et al., 2019), following the so-called "thumbprint terrain" (TPT) pattern. TPTs are characterized by sets of curvilinear features made up of continuous and discontinuous alignments of pitted domes (Figure 1). They are recognizable in several locations in the Northern hemisphere of Mars (Lockwood et al., 1992; Tanaka et al., 2014) and Arcadia Planitia is one of the main sites of this sort (Kreslavsky & Head, 2002; Lucchitta, 1981; Pomerantz & Head, 2003; Ramsdale et al., 2019; Scott & Underwood, 1991; Tanaka et al., 2005). Nonetheless, such landforms on Mars have been assigned several different interpretations. They have been linked to magmatic volcanism (Bridges et al., 2003; Bruno et al., 2004; Ghent et al., 2012; Hiesinger et al., 2009), tsunami deposits (Costard et al., 2017; Rodriguez et al., 2016), ice-related processes (Grizzaffi & Schultz, 1989; Guidat et al., 2015; Lockwood et al., 1992; Scott & Underwood, 1991), and also sedimentary volcanism has often been associated with these kinds of morphologies

Writing – review & editing: B. De Toffoli, M. Massironi, F. Mazzarini, A. Bistacchi

at several Martian locations (Ivanov et al., 2014; Oehler & Allen, 2010; Orgel et al., 2015; Skinner & Mazzini, 2009). In the specific case of Arcadia Planitia, TPT morphology has been attributed to Amazonian fluid and sediment resurgences (De Toffoli et al., 2019). The pitted mounds that characterize the region in fact display geomorphological characteristics consistent with them being eruption centers, typical thermal inertia of fine-grained loose materials, and spatial patterns highlighting their connection with subsurface fracture systems (De Toffoli et al., 2019), which would be absent whether the mounds would be the result of as ice-related and surficial processes (De Toffoli et al., 2018).

In this work, we present a complete mapping of the TPT at the study area, highlight their main geomorphological traits and spatial distribution characteristics, and finally investigate the underlying subsurface rheology using an analysis of their rooting fracture networks. These fractures, in fact, could have acted as pathways for fluid percolation during the venting process.

2. Data and Methods

We surveyed an area of ~122,000 km^2 and mapped more than 9,000 mounds, including the sample area of ~12,000 km^2 containing around 2,000 mounds previously analyzed by De Toffoli et al. (2019). To produce a reproducible work, we compiled an extensive map of all mounds and all alignments and other significant morphological constituents of the TPT, and performed cluster and fractal analyses and investigated the alignments and spacings within the TPT. These methods allowed us to test the potential relationships between these surface expressions and the underlying systems of connected fracture networks that could have acted as pathways for fluid percolation (Mazzarini & Isola, 2010).

All the observations were performed on a mosaic of 46 Mars Reconnaissance Orbiter (MRO) Context Camera (CTX) images (6 m/pixel resolution; Malin et al., 2007) produced by USGS Astrogeology service's Pilot data portal (Akins et al., 2009), and additional context information was retrieved from THEMIS thermal inertia (Night-time Infrared images: Christensen et al., 2003) data and the Mars Orbiter Laser Altimeter (MOLA; ~460 m/pixel; Smith et al., 2001; Zuber et al., 1992) topographical elevation model. Mapping and image analysis were performed with ArcGIS® using sinusoidal projections centered on the study area in order to minimize spatial distortion.

2.1. Cluster and Fractal Analyses

The fractal analysis adopted here is a statistical procedure based on the spatial distribution of point features and provides information about the connection between emission points at the surface and the subsurface sources of the ejected materials at depth (Mazzarini & Isola, 2010).

The investigation of the subsurface was performed by the application of cluster and fractal analyses to the entirety of the mapped mound population. We mapped 9,028 individual mounds in Arcadia Planitia, over an area of about 122,000 km^2. For consistency with previous work (De Toffoli et al., 2018, 2019), each feature was distinguished from its neighbors through manual identification (Pozzobon et al., 2019), and each mapped point was assigned to the mounds' summit pits. We individually mapped mounds above 100 m in diameter (i.e., characterizing traits visible at CTX resolution) and mapped alignments of single or coalescent mounds as lines. While location of each mound was defined by mapping the central pit, lines were drawn connecting the apical pits of coalescent or adjacent mounds. Where chains of coalescent mounds occurred, the summit pit location identification was supported by the observation of perimetral moats or swellings and circumferential troughs associated to the mounds in plan view.

Fractal analysis investigates the spatial properties of vents or fractures and how they fill the space. The investigation of vents, as in the framework of this study, allows us to collect information regarding the underlying fracture systems since vents represent the position of fractures that reached the surface (Mazzarini & Isola, 2010). We performed the spatial distribution analyses according to Mazzarini and Isola (2010) workflow of clustering and fractal investigation. An additional step was taken to further analyze groups of vents where the landform preservation appeared optimal (i.e., minimum erosion, dust cover, obliteration, etc.). To achieve this, independently from the first clustering technique, we also performed a second clustering methodology and subdivided part of the population into additional clusters by selecting groups of mounds

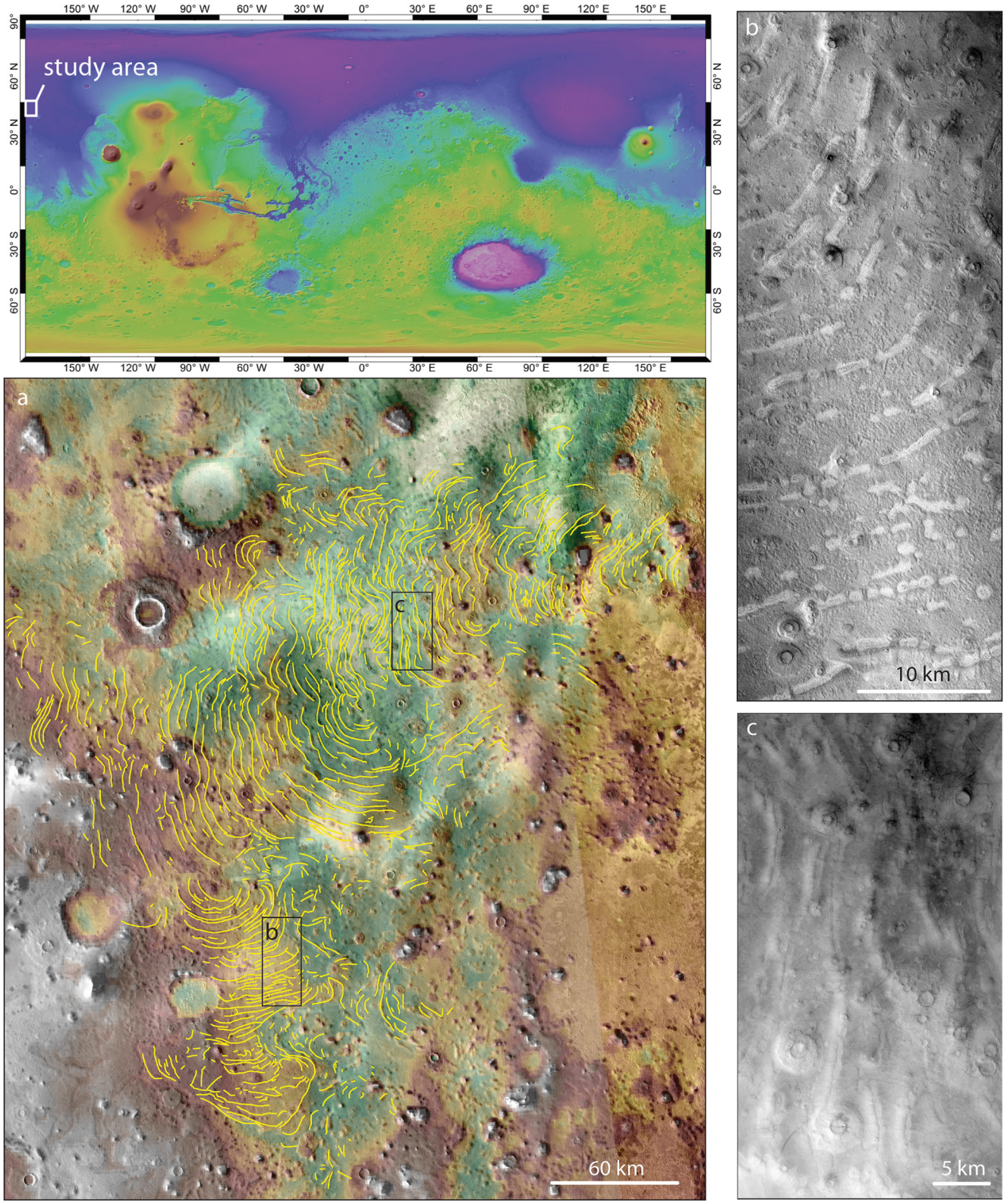

Figure 1. Overview of the study area. Thumbprint terrain (TPT) in Arcadia Planitia. (a) Mapping of the TPT, marked with yellow lines overlaid on THEMIS daytime infrared (THEMIS IR) and Mars Orbiter Laser Altimeter Digital Terrain Model (MOLA DTM) datasets. (b) Image subset of the mound alignments and (c) mound alignments arranged in curvilinear ridges and associated with bulging (Context Camera mosaic, Malin et al., 2007).

where, from a visual analysis of CTX images, minimal erosion or obliteration had occurred (cf. Figure S1 in Supporting Information S1). Subsequently, self-similar clustering (i.e., fractal) analysis was performed on each cluster. This methodology provides insights into the possible presence of hydraulic connections between mounds at the surface and potential fluid sources at depth via an underlying connected fracture network (De Toffoli et al., 2018; Mazzarini, 2007; Mazzarini & Isola, 2010). When the fracture network is a percolating system, its spatial distribution is fractal (self-similar) and is defined in a specific length-scale bounded by a lower and an upper cutoff (Lco and Uco; Mazzarini & Isola, 2010).

Fractal behavior was analyzed by applying the two-point correlation sum method (Bonnet et al., 2001 and references therein). The correlation sum ($C(l)$) is defined as $C(l) = 2\,N(l)/N(N-1)$ where $N(l)$ are the pairs of points (i.e., the locations of the mapped central pits) whose distance is less than l. If the fractal distribution exists this correlation is valid: $C(l) \sim l^D$, where D is the fractal dimension. Self-similarity (i.e., fractal behavior) occurs when a plateau is visible in a $\Delta\log(C(l)/\Delta\log(l))$ versus $\log(l)$ plot (Clauset et al., 2009; Mazzarini & Isola, 2010). The edges of the plateau define the Lco and Uco, where the Uco represents the distance between the surface and the depth of the fluid reservoirs (Mazzarini & Isola, 2010; cf. Text S1 and Figure S2 in Supporting Information S1).

We adopted error minimization procedures to obtain the best estimate for Uco values. We firstly identified the Uco depth range corresponding to the highest values of R^2 (i.e., correlation coefficient of $C(l) \sim l^D$), where R^2 is defined by the least squares method. The error of the measure was estimated by calculating half the difference between the maximum and the minimum depths (i.e., distance from the mapped surface) where the R^2 shows the best-fit value (De Toffoli et al., 2018). Additionally, for the estimates to be statistically meaningful, clusters of at least 50 samples are required to extract robust parameter estimates (Clauset et al., 2009). For large datasets (>200) removing a random sample of 20% of the vents does not significantly affect the estimate of the fractal exponent (less than 0.01% of variation) and the error introduced in the estimation of the cut-offs is less than 1%–2% (Mazzarini & Isola, 2010). It has been shown that adding random errors up to 500 m to points locations does not change the estimation of the cut-offs, as they are not statistically different from those computed for the original data set (Mazzarini et al., 2013). In our data set, the number of samples per analyzed cluster span from a minimum of 454 to a maximum of 2,073.

2.2. Fracture Spacing Analysis

Fracture spacing analysis is a statistical procedure which allows the characterization of the fracture spacing in a fracture set, defined as a set of fractures of similar orientation and genetic origin. Fracture spacing can be considered as a proxy for the thickness of a brittle layer fractured under tension (Bai et al., 2000).

We considered the mound alignments as expressions of fractures that showed tensional behavior, at least during the opening of the conduits that we suggest have allowed the fluid expulsion. We mapped 984 line features over the study area. Each line was mapped by connecting the apical pits of coalescent or adjacent mounds sitting along the same alignment. The phenomenon that this technique investigates is linked to the brittle response of rocks undergoing tensional stress. When layered materials experience extensional stress intense enough to begin cracking, joints perpendicular to the direction of the extension open (Bai & Pollard, 2000). The fracturing process evolves from an initial state, when zero joints are present in the system, to a state when it reaches so called "fracture saturation" which occurs when no new joints form and any additional strain is accommodated by further opening of the existing joints (Bai et al., 2000). At saturation, joints are organized according to a regular spatial distribution (approximately constant spacing between fractures) and the parametric distribution of spacing is close to a symmetrical normal distribution. In contrast, when fractures are randomly distributed, a parametric exponential distribution of spacing will be observed (Bistacchi et al., 2020). Intermediate situations would show asymmetrical gamma or log-normal parametric distributions (Rives et al., 1992) representing a certain degree of fracture organization evolving toward a situation of fracture saturation (Bai & Pollard, 2000; Bistacchi et al., 2020; Rives et al., 1992; Tan et al., 2014). Overall, an evolution from strongly skewed to symmetric distributions is observed with the increasing maturity (or saturation) of a joint set.

Bai et al. (2000) observed that at saturation, joint spacing tends to be of the same order of magnitude of the thickness of the fractured layer (fracture spacing/layer thickness ratio 1). Thus, the spacing distribution of

joints can be considered a proxy for (a) the degree of evolution of the system (shape of the statistical distribution) and (b) the thickness of the fractured layer. To collect spacing data, we did not use all the mapped line features, but selected portions of the study area where the totality of the lineaments was visible at the mapping resolution. This was necessary to avoid errors induced by the obliteration of fractures (e.g., obliteration due to impact debris overlay, dust deposition, lava flows and erosion), that tend to increase the apparent spacing (e.g., in a sequence of three fractures, if the middle one is hidden, the resulting spacing will be twice the real one). We selected eight regions (O1–O9. O2 resulted too small to be statistically significant and it was not possible to run any meaningful analyses. It was accordingly discarded, cf. Data Set S2 in Supporting Information S1) that fulfilled this condition of complete representation.

Since spacing is defined as the distance measured perpendicular to fractures/joints, and since TPTs are sinuous in map view, we automatically computed sets of sampling lines perpendicularly cross-cutting the TPT linear features within each region (code, figures, and complete data set Data Sets S2 and S3 in Supporting Information S1) and measured the spacing between their intersections with the TPT linear features. The sampling lines were obtained as "streamlines" perpendicular to the TPT linear features at every location. The seed points for individual streamlines were manually selected in order to avoid sampling lines with no geomorphological or statistical significance (e.g., extremely short sampling lines or large groups of sampling lines sharing common segments). Preliminary statistics were calculated for single sampling lines in order to test whether the analyses were well posed (e.g., if the region was large enough to yield significant results). When a minimum of 10 exploitable sampling lines for each region was found, we calculated cumulative statistics to combine the sampling lines into a single one, in order to obtain very long sampling lines with a large number of intersections on which to base the fracture spacing. At this stage, empiric spacing distributions can be measured for each individual region, and the parameters of best-fit parametric distributions can be calculated and used as proxies as explained above (Bistacchi et al., 2020).

3. Observations

TPTs appear as arcuate curvilinear alignments of pitted mounds with a limited relief (visible at MOLA resolution), a summit pit, a lighter relative brightness compared to the surrounding plain, perimeter moats and swellings, a rough surface, and concentric troughs surrounding the central pit (Figure 2). On Nighttime Infrared (IR) THEMIS imagery data TPTs appeared easily recognizable as dark linear and arcuate structures representing a common low thermal inertia (Farrand et al., 2005; Mellon et al., 2000; Oehler & Allen, 2010). In this area, such mounds have been interpreted as emission centers produced by subsurface sediment mobilization, venting on a large portion of the area under study (De Toffoli et al., 2019; Farrand et al., 2005; Oehler & Allen, 2010; Skinner & Mazzini, 2009; Skinner & Tanaka, 2007; Tanaka et al., 2003). TPTs thus represent highly fractured zones characterized by a dense presence of venting spots. The new mound population herein investigated includes the previously analyzed population (De Toffoli et al., 2019) and mounds in adjacent neighbourhoods, generating a total of 9,028 mapped mounds.

The TPTs appear as arcuate lineaments with a maximum length of 53 km. The alignments are also highlighted in places by surface bulging (Figure 1c). These bulges are observed more frequently in the northern part of the area and almost disappear toward the south. In the study area the bending direction of TPT alignments appear as a prominent trait of the population. In fact, the convexity of lineaments gently bends over the entire population from a E-W toward a N-S direction moving southward (Figure 1a). TPT arcuate alignments show a peculiar curvilinear trend running upslope and indicate interactions with the underlying topography, bending and disappearing where encountering topographical features characterized by higher elevation (Figure 1a).

It has already been demonstrated that a large sample of the mound population is the products of sedimentary volcanism (De Toffoli et al., 2019). At the CTX resolution, we do not observe any perceivable difference between the mounds included and excluded from the sample population, they share homogeneous key traits with very little variability. Accordingly, there is no geomorphological evidence to not assign a homogeneous interpretation to the whole mound field. Overall, their homogeneous morphology and this consistent pattern of behavior leads us to consider the TPT population to be the product of a single process, or a set of processes, that generated non-randomly distributed mound alignments over a defined area.

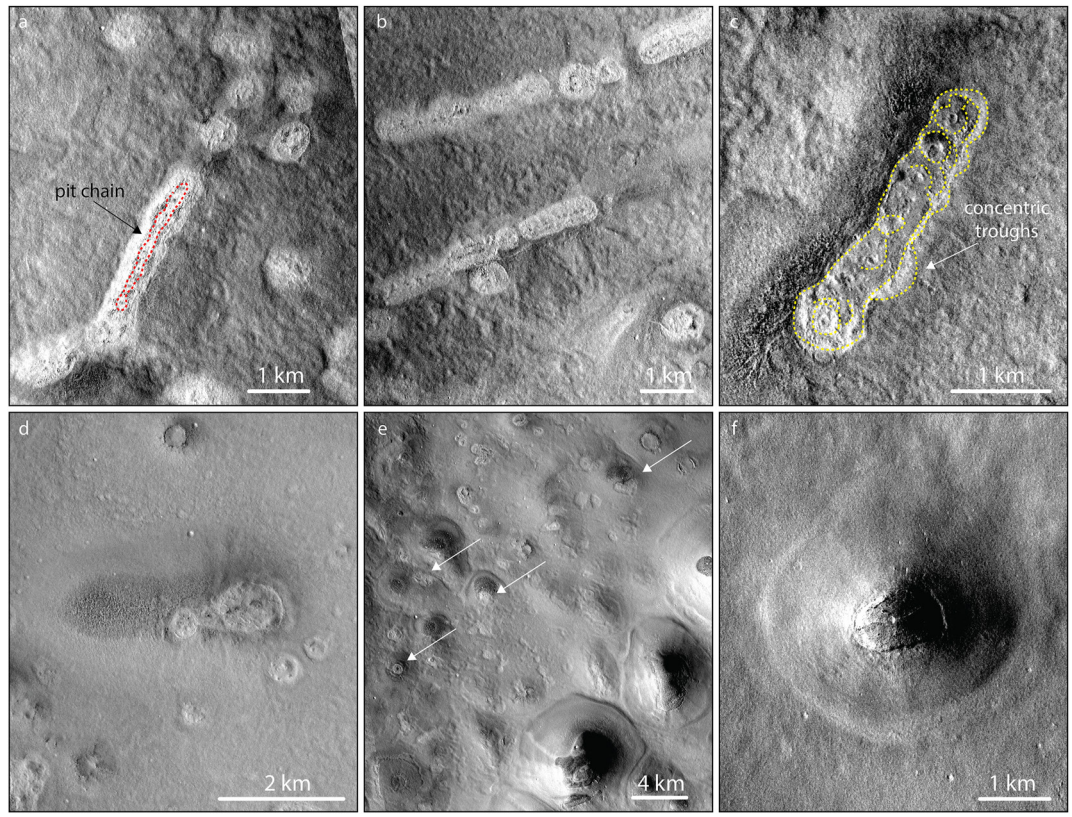

Figure 2. Example of mounds in Arcadia Planitia. (a–d) Single and aligned mounds that represent thumbprint terrains (TPTs) display characteristic features such as pits, pit chains, light relative brightness, and concentric troughs (CTX 6 m/pxl). In contrast, (d–f) mounds, that may interpreted as volcanic edifices partially covered by debris/dust accumulations, appear dark and visibly topographically higher (on Mars Orbiter Laser Altimeter elevation map) than TPT mounds (d–f). In some cases, TPTs appear to overlap the dark mounds. (d, e) They can be found in groups and have different dimensions.

4. Rheological and Mechanical Layering of the Crust

The investigation of fractures that underlie the mounds allows a better understanding of processes and conditions leading to the venting of sediments toward the surface as well as assisting the understanding of the subsurface structure. These piping systems connect the surface to the subsurface source of the erupted materials which, in sedimentary volcanism, represent layers enriched in fluids and/or loose sediments that thus constitute mechanical discontinuities. To probe the structures beneath the TPT, we hence applied fractal and fracture spacing analyses that provide information about the rheological boundaries of the underlying rocks (e.g., Bai et al., 2000; Mazzarini & Isola, 2010).

Fractal analysis highlighted three main recurrent source depth ranges beneath the TPT field: from the shallowest to the deepest, (a) 4 ± 0.2 km–4.8 ± 0.2 km; (b) 14 ± 2–23 ± 3 km; and (c) 50 ± 5–55 ± 5 km (Figure 3, cf. Table S1 and Data Set S1 in Supporting Information S1). Fracture spacing analysis suggests that the joint network is evolving toward saturation (we observed log-normal and normal distributions) and suggests an uppermost mechanical layer thickness of the same order of 4 km as the shallowest material source detected with fractal analysis (Figure 3). Arcadia Planitia is a sedimentary basin in the Martian lowlands (Tanaka et al., 2014) and the first few kilometers from the surface are likely composed of a sedimentary sequence of basin infilling with a possible partial surficial cementation due to shallow sulphate-bearing ice or brines (e.g., Cooper & Mustard, 2002; Golombek et al., 2020). This sediment pack has the potential to also represent the source of loose materials that were vented out from the mound pits in the TPT.

Deeper, we detected an intermediate source ranging from between 14 and 23 km depth. Noticeably, this interval matches the estimated range of depths of the proposed clathrate-rich cryosphere stability zone

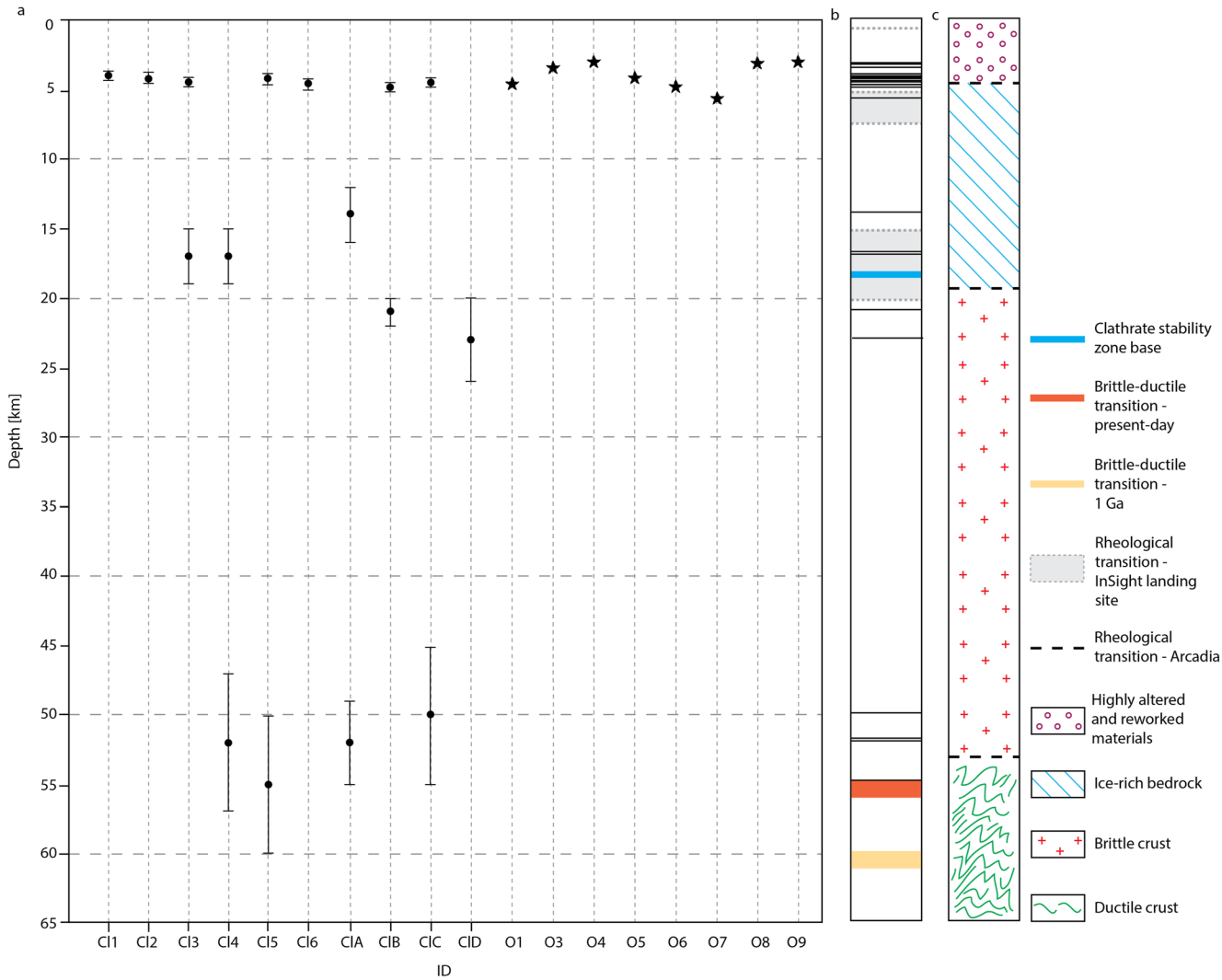

Figure 3. Results on mechanical stratigraphy. (a) Dot markers with error bars represent the estimated maximum extensions of the system of connected fractures underneath each cluster (i.e., cluster and fractal analysis outcomes); stars represent the statistically significant thickness estimate for the topmost layer obtained through the fracture spacing analysis for each region. On the right-hand side of the figure, in the left column these results are compared with (b) the base of clathrate stability zone (estimates refer to the latitude of Arcadia Planitia with a present-day-like heat flow of 15 mW m^{-2}) (Clifford et al., 2010). In blue, the brittle-ductile transition for wet rheology under present-day (in orange) and 1 Ga (in red) conditions (Azuma & Katayama, 2017). (c) In the furthest right column, the reconstruction of the rheological stratigraphy inferred from fractal and fracture spacing analyses at the study site is shown.

up to the proposed cryosphere/hydrosphere contact (Clifford et al., 2010) leading to the inference that this fracture network system had the potential to connect the source of the ejected fluids (ostensibly water resulting from ice melting or gas hydrate dissociation) to the surface. Hence, given the observed layering, we propose that the fluids were probably sourced from the deeper level and mixed with loose materials once they reached the topmost layer, which acted as an intermediate reservoir before the final discharge.

Moving deeper still, fractal analysis suggested the presence of a deep source layer located between 50 and 55 km below the surface. To crack such an extensive portion of the crust, volcanic, tectonic or impact processes must be invoked (Rossi, 2018). A single impact event, as observed in Arabia Terra (Pozzobon et al., 2019), can be excluded since there is no evidence on the surface of an impact large enough to generate a 122,000 km^2 mound field. To include the entire field, a crater of over 500 km radius should be present. Such extensive dimension is reached by major basins like Argyre, while in Arcadia there is no evidence at the surface of an impact of this magnitude. However, a combination of multiple impacts, today buried and obliterated, might have had the potential to deeply fracture the crust, generating organized fracturing that

pre-existed the TPT (e.g., arcuate patterns). Tectonic processes might also be responsible for such pervasive deep cracking. The brittle lithosphere (i.e., schizosphere) of recent Martian times (~1 Ga) is assumed to reach depths comparable to those herein observed (Azuma & Katayama, 2017; Grott & Breuer, 2008, 2010) and could have been fractured by prolonged tectonic activity (Banerdt et al., 2020; Lognonné et al., 2019). In this context, volcanic processes might also have played a role. Dark mounds that might be of magmatic origin displaying possible summit calderas (Figures 2d–2g) are also present in the area, but they appear clearly distinct from the mounds included in our analyses. Additionally, in some cases the TPT mounds appear to overlap such features (Figures 2d and 2f). In view of this, we do not favor the hypothesis that different groups of mounds (i.e., TPT) may have originated from different processes. Indeed, the brittle-ductile interface (i.e., rhizosphere-plastosphere boundary) is a rheological discontinuity which can act as a boundary where magmatic, hydrothermal and epithermal fluids can accumulate and eventually reach the surface when favorable cracking occurs.

Overall, the application of fractal and spatial analyses allowed us to identify mechanical discontinuities (i.e., materials reservoirs and brittle layer thickness) and thus reconstruct the mechanical stratification in the study area (Figure 3), providing additional support to the mechanical discontinuities of the Martian subsurface separately reported by various authors (e.g., Azuma & Katayama, 2017; Clifford et al., 2010; Giardini et al., 2020; Lognonné et al., 2020).

Martian mechanical stratification was also inferred by the NASA mission InSight (Interior Exploration using Seismic Investigations, Geodesy and Heat Transport) (Giardini et al., 2020; Lognonné et al., 2020), the first robotic mission aimed at exploring seismicity on planets other than Earth. InSight recorded seismic activity on Mars due to local perturbations, such as wind, diurnal temperature changes, and tectonism with spectral features very similar to those observed for seismic events on Earth (Giardini et al., 2020; Golombek et al., 2020). In addition, for the first time a local mechanical stratigraphy for a sector of the planet has been inferred by analyzing the propagation of the seismic waves (Giardini et al., 2020; Lognonné et al., 2020). At the InSight landing site, the stratigraphy appears to be characterized by a very thin and weak surficial regolith layer (cohesion up to 12 kPa, and Young's modulus of 0.2 GPa; Golombek et al., 2020) 10–100 m thick (Lognonné et al., 2020); an upper crust layer 5–7 km thick probably composed of regolith, sediments and highly altered and damaged basalts (with shear-wave velocity V_s 1.7–2.1 km/s) and a deeper crust layer, from 5 to 7 km to a depth of about 15–20 km, composed mainly of less altered basalts (V_s 2–3 km/s; Lognonné et al., 2020). Beneath this layer, down to 100 km depth, the crust is composed mainly of basaltic rocks (V_s 2.8–4 km/s) (Lognonné et al., 2020).

5. Wider Implications

On Earth, the thickness of different mechanical layers (i.e., sedimentary basins and brittle crust) control the scaling laws of fractures and earthquakes (e.g., Davy, 1993; Ouillon et al., 1996; Pacheco et al., 1992). In volcanic areas, the spatial distributions of both faults and vents provide a coherent image of the crustal layering as observed in the areas along the East African Rift System (e.g., Mazzarini & Isola, 2010, 2021). The fractal distribution of mounds/vents correlates well with the crust layering and structure providing the depth of the fluid source for mud volcanoes in the Greater Caucasus region in Azerbaijan (Bonini & Mazzarini, 2010). The fractal analysis of spatial distribution of vents has also been successfully applied to other areas of Mars (Pozzobon et al., 2019) as well as on icy planetary bodies, such as Enceladus and Ganymede (Lucchetti et al., 2017, 2021).

In view of the homogeneity of characterizing traits and structure distribution patterns of TPTs, the TPT constituting mounds of Arcadia Planitia are likely to have a common origin. Subsurface sediment mobilization is usually the result of the upwelling of fluids stored at depth that occurs when the buoyancy forces that push the mixtures upward exceed the confining lithostatic pressure (Kopf, 2002). This can be triggered by fluid supply, viscosity decrease or increased pore pressures that in turn could be induced by various events such as impact cratering unloading, hydrothermal pulses, tectonic loading, seismic triggers or injection of gas following clathrate dissociation (Dimitrov, 2002; Oehler and Allen, 2010; Prieto-Ballestreros et al., 2006; Skinner & Mazzini, 2009; Skinner & Tanaka, 2007). Since no unequivocal evidence distinguishing these

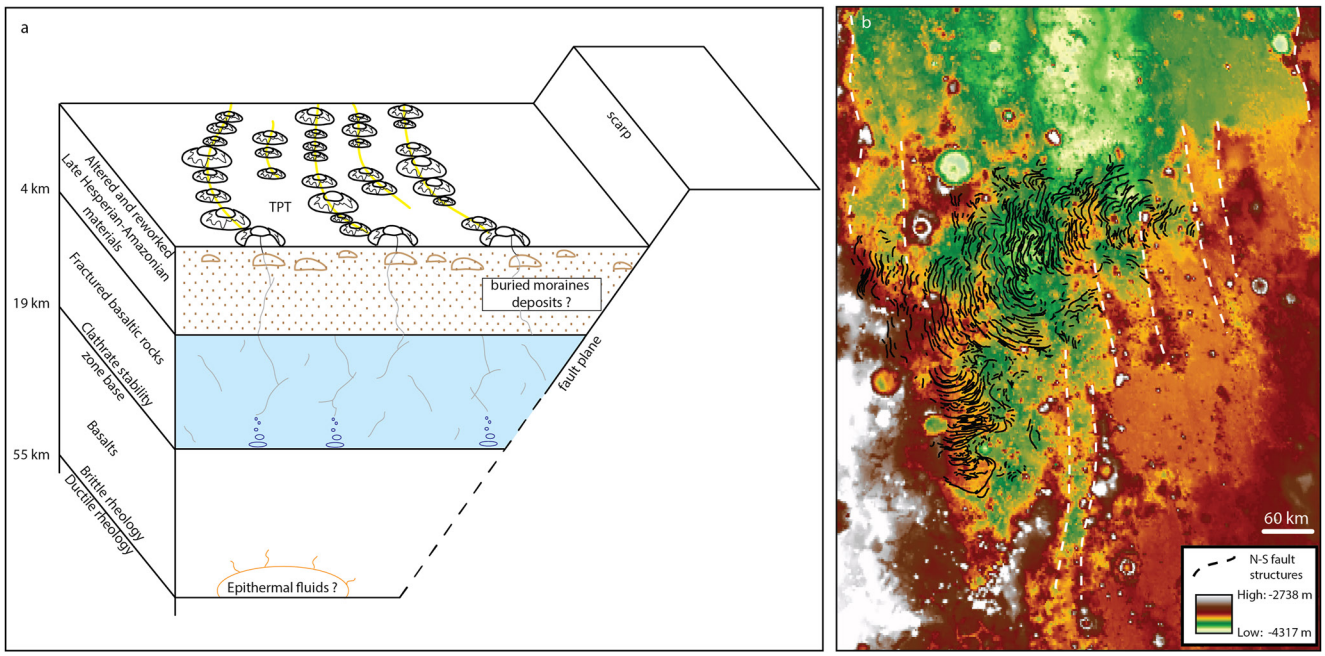

Figure 4. Overall surface-subsurface model and structural features. (a) The reconstruction of the subsurface mechanical layering, interpreted fluid and sediment reservoir locations and pathways, and putative geometrical relationship between TPT and possible N-S faults. (b) Fault traces observed in the study area are highlighted with dashed white lines while black solid traces indicate mapped thumbprint terrains.

phenomena was found from the analyses of the orbital optical imagery (e.g., faults overlapping, large volcanic/mud flows, etc.), the trigger that led to the generation of the TPTs could not be identified.

In relation to this question, we report the pervasive presence of linear structure that we interpret as faults in the study area, since this kind of feature has the potential to play a role in subsurface mobilization, given their involvement in some of the above-mentioned processes such as tectonics, liquefaction or hydrothermalism. We observed a set of N-S fault scarps at least 100 km long, characterized by ~60 m of topographic drop, around and intersecting the whole TPT population (with TPTs overlapping in places the fault traces) and located 20–90 km apart from one another (Figure 4b). It needs to be taken into account that no relationship between large-scale faults and liquefaction events has ever been previously observed on Mars. In addition, there is no proof that the observed faults were active while water/ice reservoirs were available in the Martian subsurface. Nevertheless, on Earth this connection is well established, and the link between faults and fluid-sediment resurgence is commonly observed, since material upwellings preferentially develop along pre-existing surface or near-surface discontinuities and weaknesses (e.g., Bonini et al., 2016; Manga & Brodsky, 2006; Manga et al., 2019). Excellent examples of this phenomenon are the liquefaction events related to the 2,010–2,011 Canterbury earthquake sequence in New Zealand (Quigley et al., 2013; Reid et al., 2012; Townsend et al., 2016). In this case, liquefaction occurred in areas (up to ~70 km from the epicenter) of abandoned or recently in-filled river channels, swampy ground and areas underlain by estuarine deposits; the most heavily affected areas appear to be related to near-surface alluvial features, such as channels and meander loops, filled with loose, unconsolidated sediment (Bastin et al., 2015; Cubrinovski et al., 2011; Townsend et al., 2016; Villamor et al., 2016; Wotherspoon et al., 2012). In this context, sand boils and sand volcanoes developed aligned along the pre-existing buried features, generating arcuate or straight sets of discharge vents alignments (Reid et al., 2012; Townsend et al., 2016).

On Mars, mid-latitude zones between 30° and 55°, including the Arcadia region, recorded traces of glacial features up to the late Amazonian period, such as glacier-like forms and viscous flow of ice-rich sediments capable of moving significant volumes of material, that may indicate the presence of buried moraines at the study site (Brough et al., 2019; Souness & Hubbard, 2012). In this particular case, the TPT convolute geometries might reflect the arrangement of buried moraines (e.g., Arfstrom & Hartmann, 2005) which may have provided the pre-existing points of weakness (i.e., unconsolidated debris) finally exploited as preferential

pathways by fluids and sediments to discharge to the surface after their remobilization (Figure 4a). This process might have taken place where fluids and fractures reached the surface as a result of the deeper subsurface mechanisms and rheology, which determined fracture and vent spacing.

6. Conclusions

The investigation of planetary interiors and subsurfaces is a fast-developing field, tackling largely unknown environments. On Mars, thanks to the InSight mission, a new era for planetary seismology and geology has opened, and many more discoveries are yet to come. We carried out independent analyses on chains of numerous mounds interpreted as sedimentary volcanoes, retrieving the mechanical stratigraphy for Arcadia Planitia, and compared the results obtained with the observations performed at the InSight landing site, and multiple subsurface modeling studies. Through the application of fractal and fracture-spacing analyses, we identified three mechanical discontinuities at c. 4–5, c. 14–23, and c. 50–55 km, which are in good accordance with the layering inferred from the seismic wave propagation recorded by InSight, which revealed an upper weaker layer at 4–7 km over a bedrock up to 15–20 km in depth. Our outcomes also match previous global modeling of the Mars interior that predict a cryosphere base depth at c. 18 km (Clifford et al., 2010) and a brittle lithosphere base depth comparable to the deep discontinuity observed in the present study at c. 50–55 km (Azuma & Katayama, 2017; Grott & Breuer, 2008, 2010). Further modeling and observations are needed to tackle and explain the processes that triggered, or contributed to, the formation and developed of the fracture systems and materials upwelling. An interpretation investigating the origin of the mounds might in fact provide further clues on recent water-related processes in the Martian crust.

By demonstrating the efficiency of these techniques in the field of subsurface mechanical layering reconstruction, we provide a workable tool to expand these investigations to further areas on Mars. This has the potential to significantly increase the number of case studies beyond the range of InSight, but that can assist in a global mapping of the subsurface layering of the planet.

Conflict of Interest

The authors declare no conflicts of interest relevant to this study.

Data Availability Statement

Supplementary materials have been provided as ancillary files to this paper. Large datasets have been archived in an external repository (https://doi.org/10.6084/m9.figshare.15059886.v1).

Acknowledgments
The authors thank Jason D. Ramsdale and the other anonymous reviewer for their thoughtful comments that helped to improve an earlier version of this paper. The authors also thank the editor Laurent G. J. Montesi for handling this manuscript. This paper was supported by the European Union's Horizon 2020 research and innovation program under grant agreement N°776276 (PLANMAP). The authors gratefully acknowledge the financial support and endorsement from the DLR Management Board Young Research Group Leader Program and the Executive Board Member for Space Research and Technology. The authors are grateful for the fruitful discussion with Doris Breuer, Ernst Hauber, Martin Knapmeyer, and Ana-Catalina Plesa from the InSight science team and German Aerospace Center – DLR. The authors also thank Simon Crowhurst for proofreading and language editing. Open access funding enabled and organized by Projekt DEAL.

References

Akins, S. W., Gaddis, L., Becker, K., Barrett, J., Bailen, M., Hare, T., et al. (2009). Status of the PDS unified planetary coordinates database and the planetary image locator tool (PILOT). *40th Lunar and Planetary Science Conference*. Abstract #2002.

Arfstrom, J., & Hartmann, W. K. (2005). Martian flow features, moraine-like ridges, and gullies: Terrestrial analogs and interrelationships. *Icarus*, *174*, 321–335. https://doi.org/10.1016/j.icarus.2004.05.026

Azuma, S., & Katayama, I. (2017). Evolution of the rheological structure of Mars. *Earth Planets and Space*, *69*. https://doi.org/10.1186/s40623-016-0593-z

Bai, T., & Pollard, D. D. (2000). Fracture spacing in layered rocks: A new explanation based on the stress transition. *Journal of Structural Geology*, *22*, 43–57. https://doi.org/10.1016/s0191-8141(99)00137-6

Bai, T., Pollard, D. D., & Gao, H. (2000). Explanation for fracture spacing in layered materials. *Nature*, *403*, 753–756. https://doi.org/10.1038/35001550

Banerdt, W. B., Smrekar, S. E., Banfield, D., Giardini, D., Golombek, M., Johnson, C. L., et al. (2020). Initial results from the InSight mission on Mars. *Nature Geoscience*, *13*, 183–189. https://doi.org/10.1038/35001550

Bastin, S. H., Quigley, M. C., & Bassett, K. (2015). Paleoliquefaction in Christchurch, New Zealand. *The Geological Society of America Bulletin*, *127*, 1348–1365. https://doi.org/10.1130/B31174.1

Bistacchi, A., Mittempergher, S., Martinelli, M., & Storti, F. (2020). On a new robust workflow for the statistical and spatial analysis of fracture data collected with scanlines (or the importance of stationarity). *Solid Earth*, 1–18. https://doi.org/10.5194/se-2020-83

Bonini, M., & Mazzarini, F. (2010). Mud volcanoes as potential indicators of regional stress and pressurized layer depth. *Tectonophysics*, *494*, 32–47. https://doi.org/10.1016/j.tecto.2010.08.006

Bonini, M., Rudolph, M. L., & Manga, M. (2016). Long- and short-term triggering and modulation of mud volcano eruptions by earthquakes. *Tectonophysics*, *672–673*, 190–211. https://doi.org/10.1016/j.tecto.2016.01.037

Bonnet, E., Bour, O., Odling, N. E., Davy, P., Main, I., Cowie, P., & Berkowitz, B. (2001). Scaling of fracture system in geological media. *Reviews of Geophysics*, *39*, 347–383. https://doi.org/10.1029/1999RG000074

Bridges, J. C., Seabrook, A. M., Rothery, D. A., Kim, J. R., Pillinger, C. T., Sims, M. R., et al. (2003). Selection of the landing site in Isidis Planitia of Mars probe Beagle 2. *Journal of Geophysical Research*, *108*, 1–17. https://doi.org/10.1029/2001JE001820

Brough, S., Hubbard, B., & Hubbard, A. (2019). Area and volume of mid-latitude glacier-like forms on Mars. *Earth and Planetary Science Letters*, *507*, 10–20. https://doi.org/10.1016/j.epsl.2018.11.031

Bruno, B. C., Fagents, S. A., Thordarson, T., Baloga, S. M., & Pilger, E. (2004). Clustering within rootless cone groups on Iceland and Mars: Effect of nonrandom processes. *Journal of Geophysical Research: Planets*, *109*, 1–11. https://doi.org/10.1029/2004JE002273

Christensen, P. R., Bandfield, J. L., Bell, J. F., Gorelick, N., Hamilton, V. E., Ivanov, A., et al. (2003). Morphology and composition of the surface of Mars: Mars Odyssey THEMIS results. *Science*, *300*, 2056–2061. https://doi.org/10.1126/science.1080885

Clauset, A., Rohilla Shalizi, C., & Newman, M. E. J. (2009). Power-law distributions in empirical data. *SIAM Review*, *51*, 661–703. https://doi.org/10.1214/13-AOAS710

Clifford, S. M., Lasue, J., Heggy, E., Boisson, J., McGovern, P., & Max, M. D. (2010). Depth of the Martian cryosphere: Revised estimates and implications for the existence and detection of subpermafrost groundwater. *Journal of Geophysical Research*, *115*, E07001. https://doi.org/10.1029/2009JE003462

Cooper, C. D., & Mustard, J. F. (2002). Spectroscopy of loose and cemented sulfate-bearing soils: Implications for duricrust on Mars, *Icarus*, *158*(1), 42–55, https://doi.org/10.1006/icar.2002.6874

Costard, F., Séjourné, A., Kelfoun, K., Clifford, S., Lavigne, F., Di Pietro, I., & Bouley, S. (2017). Modeling tsunami propagation and the emplacement of thumbprint terrain in an early Mars ocean. *Journal of Geophysical Research: Planets*, *122*, 1–649. https://doi.org/10.1002/2016JE005230

Cubrinovski, M., Bray, J. D., Taylor, M., Giorgini, S., Bradley, B. A., Wotherspoon, L., & Zupan, J. (2011). Soil liquefaction effects in the central business district during the February 2011 Christchurch Earthquake. *Seismological Research Letters*, *82*:893–904. https://doi.org/10.1785/gssrl.82.6.893

Davy, P. (1993). On the frequency-length distribution of the San Andreas fault system. *Journal of Geophysical Research*, *98*, 12141–12151. https://doi.org/10.1029/93JB00372

De Toffoli, B., Pozzobon, R., Massironi, M., Mazzarini, F., Conway, S., & Cremonese, G. (2019). Surface expressions of subsurface sediment mobilization rooted into a gas hydrate-rich cryosphere on Mars. *Scientific Reports*, *9*, 8603. https://doi.org/10.1038/s41598-019-45057-7

De Toffoli, B., Pozzobon, R., Mazzarini, F., Orgel, C., Massironi, M., Giacomini, L., et al. (2018). Estimate of depths of source fluids related to mound fields on Mars. *Planetary and Space Science*, 1–10. https://doi.org/10.1016/j.pss.2018.07.005

Dimitrov, L. (2002). Mud volcanoes – The most important pathways for degassing deeply buried sediments. *Earth-Science Reviews*, *59*, 49–76. https://doi.org/10.1016/S0012-8252(02)00069-7

Farrand, W. H., Gaddis, L. R. & Keszthelyi, L. (2005). Pitted cones and domes on Mars: Observations in Acidalia Planitia and Cydonia Mensae using MOC, THEMIS, and TES data. *Journal of Geophysical Research: Planets*, *110*, 1–14. https://doi.org/10.1029/2004JE002297

Ghent, R. R., Anderson, S. W., & Pithawala, T. M. (2012). The formation of small cones in Isidis Planitia, Mars through mobilization of pyroclastic surge deposits. *Icarus*, *217*, 169–183. https://doi.org/10.1016/j.icarus.2011.10.018

Giardini, D., Lognonné, P., Banerdt, W. B., Pike, W. T., Christensen, U., Ceylan, S., et al. (2020). The seismicity of Mars. *Nature Geoscience*, *13*, 205–212. https://doi.org/10.1038/s41561-020-0539-8

Golombek, M., Warner, N. H., Grant, J. A., Hauber, E., Ansan, V., Weitz, C. M., et al. (2020). Geology of the InSight landing site on Mars. *Nature Communications*. https://doi.org/10.1038/s41467-020-14679-1

Grizzaffi, P. & Schultz, P. H. (1989). Isidis Basin: Site of ancient volatile-rich debris layer. *Icarus*, *77*, 358–381. https://doi.org/10.1016/0019-1035(89)90094-8

Grott, M., & Breuer, D. (2008). The evolution of the Martian elastic lithosphere and implications for crustal and mantle rheology. *Icarus*, *193*, 503–515. https://doi.org/10.1016/j.icarus.2007.08.015

Grott, M., & Breuer, D. (2010). On the spatial variability of the Martian elastic lithosphere thickness: Evidence for mantle plumes? *Journal of Geophysical Research*, *115*, 1–16. https://doi.org/10.1029/2009JE003456

Guidat, T., Pochat, S., Bourgeois, O., & Souček, O. (2015). Landform assemblage in Isidis Planitia, Mars: Evidence for a 3 Ga old polythermal ice sheet. *Earth and Planetary Science Letters*, *411*, 253–267. https://doi.org/10.1016/j.epsl.2014.12.002

Hiesinger, H., Rohkamp, D., & Sturm, S. F. (2009). Geology, ages, morphology, and morphometry of thumbprint terrain in Isidis Planitia, Mars. *Lunar and Planetary Science Conference*, *6*, 4–5.

Ivanov, M. A., Hiesinger, H., Erkeling, G., & Reiss, D. (2014). Mud volcanism and morphology of impact craters in Utopia Planitia on Mars: Evidence for the ancient ocean. *Icarus*, *228*, 121–140. https://doi.org/10.1016/j.icarus.2013.09.018

Kopf, A. (2002). Significance of mud volcanism. *Reviews of Geophysics*, *40*, 1005. https://doi.org/10.1029/2000RG000093

Kreslavsky, M. A., & Head, J. W. (2002). Fate of outflow channel effluents in the northern lowlands of Mars: The Vastitas Borealis Formation as a sublimation residue from frozen ponded bodies of water. *Journal of Geophysical Research*, *107*, 5121. https://doi.org/10.1029/2001JE001831

Lockwood, J. F., Kargel, J. S., & Strom, R. B. (1992). Thumbprint terrain on the northern plains: A glacial hypothesis. *Lunar and Planetary Science Conference*, *23*, 795–796.

Lognonné, P., Banerdt, W. B., Giardini, D., Pike, W. T., Christensen, U., Laudet, P., et al. (2019). SEIS: Insight's seismic experiment for internal structure of Mars. *Space Science Reviews*. https://doi.org/10.1007/s11214-018-0574-6

Lognonné, P., Banerdt, W. B., Pike, W. T., Giardini, D., Christensen, U., Garcia, R. F., et al. (2020). Constraints on the shallow elastic and anelastic structure of Mars from InSight seismic data. *Nature Geoscience*, *13*, 213–220. https://doi.org/10.1038/ngeo256

Lucchetti, A., Pozzobon, R., Mazzarini, F., Cremonese, G., & Massironi, M. (2017). Brittle ice shell thickness of Enceladus from fracture distribution analysis. *Icarus*, *297*, 252–264. https://doi.org/10.1016/j.icarus.2017.07.009

Lucchetti, A., Rossi, C., Mazzarini, F., Pajola, M., Pozzobon, R., Massironi, M., & Cremonese, G. (2021). Equatorial grooves distribution on Ganymede: Length and self-similar clustering analysis. *Planetary and Space Science*, *195*, 105140, https://doi.org/10.1016/j.pss.2020.105140

Lucchitta, B. K. (1981). Mars and Earth: Comparison of cold-climate features. *Icarus*, *45*, 264–303. https://doi.org/10.1016/0019-1035(81)90035-X

Malin, M. C., Bell, J. F., III, Cantor, B. A., Caplinger, M. A., Calvin, W. M., Todd Clancy, R., et al. (2007). Context Camera investigation on board the Mars Reconnaissance Orbiter. *Journal of Geophysical Research*, *112*, E05S04, https://doi.org/10.1029/2006JE002808

Manga, M., & Brodsky, E. (2006). Seismic triggering of eruptions in the far field: Volcanoes and Geysers. *Annual Review of Earth and Planetary Sciences*, *34*, 263–291. https://doi.org/10.1146/annurev.earth.34.031405.125125

Manga, M., Zhai, G., & Wang, C. Y. (2019). Squeezing marsquakes out of groundwater. *Geophysical Research Letters*, *46*, 6333–6340. https://doi.org/10.1029/2019GL082892

Mazzarini, F. (2007). Vent distribution and crustal thickness in stretched continental crust: The case of the Afar Depression (Ethiopia). *Geosphere*, *3*, 152–162. https://doi.org/10.1130/GES00070.1

Mazzarini, F., & Isola, I. (2010). Monogenetic vent self-similar clustering in extending continental crust: Examples from the East African Rift System. *Geosphere*, *6*, 567–582. https://doi.org/10.1130/GES00569.1

Mazzarini, F., & Isola, I. (2021). Vent distribution and structural inheritance in an embryonic rift: The example of the Chyulu Hills off-rift magmatic range (South Kenya). *Journal of Volcanology and Geothermal Research*, *416*, 107268. https://doi.org/10.1016/j.jvolgeores.2021.107268

Mazzarini, F., Keir, D., & Isola, I. (2013). Spatial relationship between earthquakes and volcanic vents in the central-northern Main Ethiopian Rift. *Journal of Volcanology and Geothermal Research*, *262*, 123–133. https://doi.org/10.1016/j.jvolgeores.2013.05.007

Mellon, M., Jackosky, B. M., Kieffer, H. H., & Christensen, P. R. (2000). High-resolution thermal inertia mapping from the mars global surveyor thermal emission spectrometer. *Icarus*, *148*, 437–455. https://doi.org/10.1006/icar.2000.6503

Oehler, D. Z., & Allen, C. C. (2010). Evidence for pervasive mud volcanism in Acidalia Planitia, Mars. *Icarus*, *208*, 636–657. https://doi.org/10.1016/j.icarus.2010.03.031

Orgel, C., Hauber, E., Skinner, J. A., Gasselt, S. V., Ramsdale, J., Balme, M., et al. (2015). Distribution, origin and evolution of hypothesized mud volcanoes, thumbprint terrain and giant polygons in Acidalia, Utopia and Arcadia Planitae: Implications for sedimentary processes in the northern lowlands of Mars. In *Lunar and Planetary Science Conference*. https://doi.org/10.1002/2014JE004682

Ouillon, G., Castaing, C., & Sornette, D. (1996). Hierarchical geometry of faulting. *Journal of Geophysical Research*, *101*, 5477–5487. https://doi.org/10.1029/95JB02242

Pacheco, J. F., Scholz, C. H., & Sikes, L. R. (1992). Change in the frequency-size relationship from small to large earthquakes. *Nature*, *355*, 71–73. https://doi.org/10.1038/355071a0

Pomerantz, W. J., & Head, J. W. (2003). Thumbprint terrain and sinuous troughs with medial ridges in the northern lowlands of Mars: Assessment of the glacial hypothesis using new spacecraft. *Lunar and Planetary Science Conference*, *34*, 1277.

Pozzobon, R., Mazzarini, F., Massironi, M., Rossi, A. P., Pondrelli, M., Cremonese, G., & Marinangeli, L. (2019). Fluids mobilization in Arabia Terra, Mars: Depth of pressurized reservoir from mounds self-similar clustering. *Icarus*, *321*, 938–959. https://doi.org/10.1016/j.icarus.2018.12.023

Prieto-Ballesteros, O., Kargel, J. S., Fairen, A. G., Fernández-Remolar, D. C., Dohm, J. M., & Amils, R. (2006). Interglacial clathrate destabilization on Mars: Possible contributing source of its atmospheric methane. *Geology*, *34*, 149. https://doi.org/10.1130/G22311.1

Quigley, M. C., Bastin, S., & Bradley, B. A. (2013). Recurrent liquefaction in Christchurch, New Zealand, during the Canterbury earthquake sequence. *Geology*, *41*, 419–422. https://doi.org/10.1130/G33944.1

Ramsdale, J. D., Balme, M. R., Gallagher, C., Conway, S. J., Smith, I. B., Hauber, E., & Wilson, J. T. (2019). Grid mapping the northern plains of mars: Geomorphological, radar, and water-equivalent hydrogen results from Arcadia Plantia. *Journal of Geophysical Research: Planets*, *124*, 504–527. https://doi.org/10.1029/2018JE005665

Reid, C. M., Thompson, NK., Irvine, J. R. M., & Laird, T. L. (2012). Sand volcanoes in the Avon–Heathcote Estuary produced by the 2010–2011 Christchurch Earthquakes: Implications for geological preservation and expression. *New Zealand Journal of Geology and Geophysics*, *55*(3), 249–254. https://doi.org/10.1080/00288306.2012.674051

Rives, T., Razack, M., Petit, J.-P., & Rawnsley, K. D. (1992). Joint spacing: Analogue and numerical simulations. *Journal of Structural Geology*, *14*(8–9), 925–937. https://doi.org/10.1016/0191-8141(92)90024-Q

Rodriguez, J. A. P., Fairén, A. G., Tanaka, K. L., Zarroca, M., Linares, R., Platz, T., et al. (2016). Tsunami waves extensively resurfaced the shorelines of an early Martian ocean. *Scientific Reports*, *6*, 25106. https://doi.org/10.1038/srep25106

Rossi, A. P. (Eds.) (2018). *Planetary Geology*. https://doi.org/10.1007/978-3-319-65179-8

Scott, D. H., & Underwood, J. R. (1991). Mottled terrain: A continuing Martian enigma. *Lunar and Planetary Science* (pp. 627–634).

Skinner, J. A., & Mazzini, A. (2009). Martian mud volcanism: Terrestrial analogs and implications for formational scenarios. *Marine and Petroleum Geology*, *26*, 1866–1878. https://doi.org/10.1016/j.marpetgeo.2009.02.006

Skinner, J. A., & Tanaka, K. L. (2007). Evidence for and implications of sedimentary diapirism and mud volcanism in the southern Utopia highland–lowland boundary plain, Mars. *Icarus*, *186*, 41–59. https://doi.org/10.1016/j.icarus.2006.08.013

Smith, D. E., Zuber, M. T., Frey, H. V., Garvin, J. B., Head, J. W., Muhleman, D. O., et al. (2001). Mars Orbiter Laser Altimeter: Experiment summary after the first year of global mapping of Mars. *Journal of Geophysical Research*, *106*, 23689–23722. https://doi.org/10.1029/2000JE001364

Souness, C., & Hubbard, B. (2012). Mid-latitude glaciation on mars. *Progress in Physical Geography*, *36*, 238–261. https://doi.org/10.1177/0309133312436570

Tan, Y., Johnston, T., & Engelder, T. (2014). The concept of joint saturation and its application. *The American Association of Petroleum Geologists Bulletin*, *98*(11), 2347–2364. https://doi.org/10.1306/06231413113

Tanaka, K. L., Robbins, S. J., Fortezzo, C. M., Skinner, J. A., & Hare, T. M. (2014). The digital global geologic map of Mars: Chronostratigraphic ages, topographic and crater morphologic characteristics, and updated resurfacing history. *Planetary and Space Science*, *95*, 11–24. https://doi.org/10.1016/j.pss.2013.03.006

Tanaka, K. L., Skinner,J. A., & Hare, T. M. (2005). *Geologic map of the northern plains of Mars*. U.S. Geological Survey, Scientific Investigations Map 2888.

Tanaka, K. L., Skinner, J. A., Jr, Hare,T. M., Joyal, T., & Wenker, A. (2003). Resurfacing history of the northern plains of Mars based on geologic mapping of Mars Global Surveyor data. *Journal of Geophysical Research*, *108*(E4), 8043, https://doi.org/10.1029/2002JE001908

Townsend, D., Lee, J. M., Strong, D. T., Jongens, R., Smith Lyttle, B., Ashraf, S., et al. (2016). Mapping surface liquefaction caused by the September 2010 and February 2011 Canterbury earthquakes: A digital dataset. *New Zealand Journal of Geology and Geophysics*, *59*(4), 496–513. https://doi.org/10.1080/00288306.2016.1182929

Villamor, P., Almond, P., Tuttle, M. P., Giona-Bucci, M., Langridge, R. M., Clark, K., et al. (2016). Liquefaction features produced by the 2010–2011 Canterbury earthquake sequence in southwest Christchurch, New Zealand, and preliminary assessment of paleoliquefaction features. *Bulletin of the Seismological Society of America*, *106*(4), 1747–1771. https://doi.org/10.1785/0120150223

Wotherspoon, L. M., Pender, M. J., & Orense, R. P. (2012). Relationship between observed liquefaction at Kaiapoi following the 2010 Darfield earthquake and former channels of the Waimakariri River. *Engineering Geology*, *125*, 45–55.

Zuber, M. T., Smith, D. E., Solomon, S. C., Muhleman, D. O., Head, J. W., Garvin, J. B., et al. (1992). The Mars Observer laser altimeter investigation. *Journal of Geophysical Research*, *97*, 7781–7797, https://doi.org/10.1029/92JE00341

References From the Supporting Information

Capozzi, R., & Picotti, V. (2002). Fluid migration and origin of a mud volcano in the Northern Apennines (Italy): The role of deeply rooted normal faults. *Terra Nova*, *14*, 363–370. https://doi.org/10.1046/j.1365-3121.2002.00430.x

Etiope, G. (2015). *Natural gas seepage. The Earth's hydrocarbon degassing*. Springer International Publishing. https://doi.org/10.1007/978-3-319-14601-0

Etiope, G., & Martinelli, G. (2009). "Pieve Santo Stefano" is not a mud volcano: Comment on "structural controls on a carbon dioxide-driven mud volcano field in the Northern Apennines" (by Bonini, 2009). *Journal of Structural Geology*, *31*, 1270–1271. https://doi.org/10.1016/j.jsg.2009.06.009

Kopf, A. (2008). Making calderas from mud. *Nature Geoscience*, *1*, 500–501. https://doi.org/10.1038/ngeo256

Mazzini, A., & Etiope, G. (2017). Mud volcanism: An updated review. *Earth-Science Reviews*, *168*, 81–112. https://doi.org/10.1016/j.earscirev.2017.03.001

Mazzini, A., Nermoen, A., Krotkiewski, M., Podladchikov, Y., Planke, S., & Svensen, H. (2009). Strike-slip faulting as a trigger mechanism for overpressure release through piercement structures. Implications for the Lusi mud volcano, Indonesia. *Marine and Petroleum Geology*, *26*, 1751–1765. https://doi.org/10.1016/j.marpetgeo.2009.03.001

Viola, G., Andreoli, M., Ben-Avraham, Z., Stengel, I., & Reshef, M. (2005). Offshore mud volcanoes and onland faulting in southwestern Africa: Neotectonic implications and constraints on the regional stress field. *Earth and Planetary Science Letters*, *231*, 147–160. https://doi.org/10.1016/j.epsl.2004.12.001